JOURNAL OF SPACECRAFT AND ROCKETS
Vol. 44, No. 4, July–August 2007

Computational Analysis of Automated Transfer Vehicle Reentry Flow and Explosion Assessment

D. E. Boutamine*
ESA, Noordwijk, The Netherlands
Ph. Reynier† and R. Schmehl†
Advanced Operations and Engineering Services, Leiden, The Netherlands
and
L. Marraffa* and J. Steelant*
ESA, Noordwijk, The Netherlands

DOI: 10.2514/1.27610

At the end of its mission to the International Space Station, during its reentry into Earth atmosphere, the automated transfer vehicle is subject to high heat fluxes leading to structural heating and fragmentation of the vehicle. It has been concluded that, depending on the mode of release, onboard residual hypergolic propellants may ignite and explode upon exposure to the hot and reactive flow environment. Because an earlier explosion of the vehicle would change drastically the impact footprint of its fragments onto the Earth surface, this study proposes a reassessment of the explosion potential. From the trajectory analysis, several points of the reentry path have been computed using a Navier–Stokes solver accounting for nonequilibrium effects. Numerical simulations have been performed with and without perforation of the structure. In parallel, a comprehensive literature survey on ignition of monomethyl hydrazine and dimethyl hydrazine vapors with pure air or air mixed with nitrogen tetroxide has been performed to assess the autoignition potential of the mixture. Finally, the results of the computational fluid dynamics computations have been used to estimate the explosion risk in the presence of a propellant leakage. Analysis confirms the risk of a destruction of the automated transfer vehicle at higher altitude, which could induce a different footprint of the fragments on the ground.

Nomenclature

A	=	area of the fissure, m^2
B	=	ballistic coefficent, $B = m/DC_d$
C_d	=	drag coefficient
c	=	sound speed, m/s
D	=	base diameter, m
dt	=	time step, s
j	=	step for the Mach number integration
M	=	Mach number
M	=	molar mass, kg
m	=	vehicle mass, kg
$\dot{m}$	=	mass flow rate, kg/s
P	=	static pressure, Pa
$p_{i,\min}$	=	minimum ignition pressure, Pa
R	=	universal gas constant, J/K/mol
r	=	gas constant per mole, J/K/kg
T	=	temperature, K
t_1	=	time duration of the supersonic flow, s
t_2	=	time duration of the subsonic flow, s
t_{ign}	=	ignition delay, s
v	=	volume of the vehicle, m^3
X	=	volume concentration
y^+	=	dimensionless value of the wall distance
γ	=	ratio of the gas specific heats
ΔH	=	enthalpy of combustion, kJ/mol
ρ	=	density, kg/m^3

Subscripts

i	=	total variable
1	=	variable upstream of the bow shock
2	=	variable downstream of the bow shock
3	=	variable inside the vehicle
*	=	variable at the fissure location

Introduction

SINCE the 1990s, the European Space Agency has conducted different studies focusing on debris engendered by space activities. These investigations were related to two main topics. The first one is coordinated by the ESOC (European Space Observation Centre) and concerns the reentry of spacecraft at the end of their mission [1–3]. The other is related to the Ariane 5 launcher and several studies have been performed by the Centre National d'Etudes Spatiales and ESA with the objective to vent propellant tanks into space at the end of the launch, thus preventing tank explosion due to solar heating [4–6]. To achieve this, tank propellants are vented into space through tubing and nozzle and submitted to a high depressurization [7]. This process can be accompanied by physical phenomena such as condensation [8,9] or vaporization [5]. One of the key points of these studies was always the prediction of the thermodynamic behavior of propellants during the venting into space. Here the topic is not to proceed to a tank passivation but to analyze the risk of vehicle explosion along its reentry trajectory path. The intensity and the altitude of vehicle fragmentation are two important parameters to assess the impact of debris on ground.

The automated transfer vehicle (ATV) is a supply cargo for the International Space Station (ISS), constituted of two elements. The first one is the spacecraft subassembly (SCS) equipped with propulsion (propulsion tanks and thrusters) and avionics bays (batteries, gyroscopes, and harness). The second part is the integrated cargo carrier, containing the equipped external bay (water and gas tanks, web structure) and the equipped pressurized module (containers, cargo, and the attitude control thrusters). A view of the spacecraft is shown in Fig. 1.

Received 1 September 2006; revision received 16 March 2007; accepted for publication 19 March 2007.

*Research Engineer, European Space Research and Technology Center.
†Research Engineer, Mechanical Engineering Business Unit.

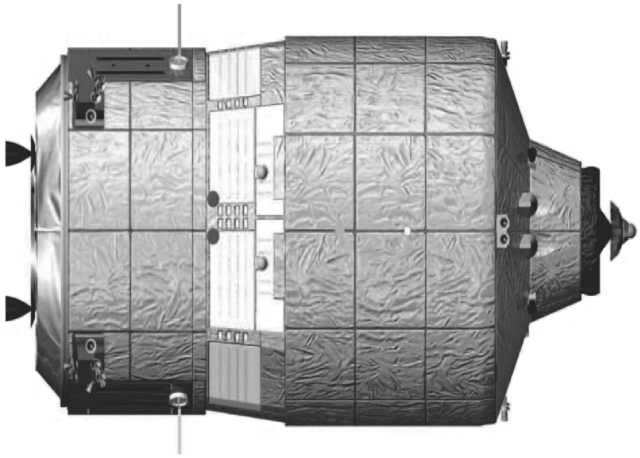

Fig. 1 Side view of the ATV (solar panels clipped off): service module (left) and integrated cargo carrier (right) [34].

At the end of its mission to ISS, ATV performs a ballistic reentry into Earth atmosphere. The vehicle is exposed to a hypersonic flow associated to high heat loads leading to the structural heating and the fragmentation of the vehicle. This process produces a high number of fragments, some of them burning up during the reentry and the others falling in the southern Pacific ocean [10]. It has been concluded that residual hypergolic propellants remaining in the SCS may ignite and explode upon exposure to the hot and reactive flow environment. Depending on the location and type of explosion, this could lead to a sudden destruction of ATV at higher altitude than expected, modifying significantly the impact footprint of vehicle fragments on Earth, with potential implications for the safety of the population on ground.

This study proposes a refined assessment of the explosion potential during ATV reentry, taking into account a perforation of the spacecraft in the presence of a propellant leakage. A detailed trajectory analysis has been performed and an estimate of the ATV destruction location has been assessed with engineering tools [11]. From the present study, several trajectory points have been selected to refine this engineering study using numerical simulations coupled to an explosion analysis. For the selected trajectory points, the flowfield around the vehicle has been simulated, using the code TAU [12] developed by DLR (German Aerospace Center). Accounting for chemical nonequilibrium and catalysis, these numerical simulations have provided the heat-flux distribution over the surface of the vehicle.

Using these results and supposing that a fissure may occurs on the vehicle structure, its most probable location can be estimated. The perforation of the body structure is assumed to occur at the location of the maximum of heat flux. In a second step, the computational domain has been extended to the interior of the vehicle, including the connecting gap in the vehicle body. The corresponding computational fluid dynamics (CFD) simulations provide the internal temperature, pressure, and species distributions accounting for dissociation and recombination reactions.

In parallel, the potential of propellant ignition and explosion has been assessed by means of qualitative and quantitative data from literature [13–16]. Correlations for minimum autoignition pressure and temperature, as well as for ignition delay times have been derived for various reaction sets. Finally, for potential scenarios of propellant leakage, the results obtained with the numerical simulations are coupled to the explosion model for assessing the ignition risk along the trajectory.

This study has been partially presented in [17].

Approach

To assess the risk of explosion during reentry, the following approach has been developed [17,18]. The main objective is to refine the engineering study [11] performed on ATV destruction. To achieve such a goal, different aspects have to be considered. A first point is to analyze the trajectory for providing the computational conditions for the CFD code in terms of pressure, temperature, density, and velocity. In a second step, the flowfield around the vehicle is computed to predict the heat-flux distribution over the surface. A fissure is then located of the heat-flux maximum and both external and internal flowfields calculated. In parallel, an explosion analysis has been developed for investigating the critical conditions to ignite an explosion of the onboard propellants. Finally, this explosion analysis is coupled to the flowfield predictions to analyze the risk of explosion assuming a leakage of the onboard residual propellants.

From the CFD point of view, the main critical aspect is the validity of an approach in which a steady flowfield is computed at different trajectory locations. This means that the dynamic aspect of the reentry, with the change in atmospheric conditions is not accounted for and that the trajectory is supposed to be, at a first approximation, a succession of steady states. The transient aspect of the flow at fissure opening, where some air in chemical nonequilibrium enters into the vehicle, is not taken into account. These assumptions are valid only if the timescale of the ATV filling by the external gas is negligible, compared to the time required to have a large change in the external conditions. To establish the validity of the approach, the filling time of the vehicle is estimated at the first order using an engineering method.

Trajectory Analysis

The reentry trajectory of the ATV has been analyzed for several cases. Four options were investigated [11], for nominal and nonnominal ATV and for a controlled and noncontrolled entry. The four cases are the following combinations:

1) Nonnominal and uncontrolled;
2) Nonnominal and controlled;
3) Nominal and uncontrolled;
4) Nominal and controlled.

The nominal reentry is related to the ATV filled with ISS waste and propellant residuals, whereas the nonnominal case refers to an uncompleted docking; that is, the down cargo (during the reentry) is the up cargo, which includes a significant amount of unused propellants. In the nonnominal case, the ATV carries about 2000 kg more mass than in the nominal one. As a consequence, the center of mass and the moment of inertia are different, which influences significantly the flight path during reentry. The noncontrolled entry is without any correction of trajectory. For the controlled entry, the ATV is oriented to perform a ballistic reentry, and the trajectory is controlled by generating an angular velocity with a pitch rate of 10 deg per second provoking a tumbling. The scenario retained for the ATV end of mission is the noncontrolled option without tumbling. Therefore, in this study the analysis is restricted for a nominal ATV performing a noncontrolled entry.

ATV destruction has been already investigated [11] using engineering methods. According to this work, ATV looses its solar arrays at 92 km of altitude, the main fragmentation is supposed to occur at 75 km [10]. In an attempt to refine this prediction, the explosion risk of ATV is assessed in the current work for two trajectory points corresponding to the altitudes of 75 and 80 km. The main characteristics of these two trajectory points, computed at the European Space Research and Technology Center (ESTEC) using the available data for the trajectory input [10,11], are reported in Table 1. The altitude evolution versus time along the trajectory is

Table 1 Free stream parameters used for the computations at the two selected trajectory points

Altitude, km	75	80
Pressure, Pa	2.35	1.05
Density, kg/m^3	3.9×10^{-5}	1.85×10^{-5}
Temperature, K	208	198.7
Velocity, m/s	7175	7202

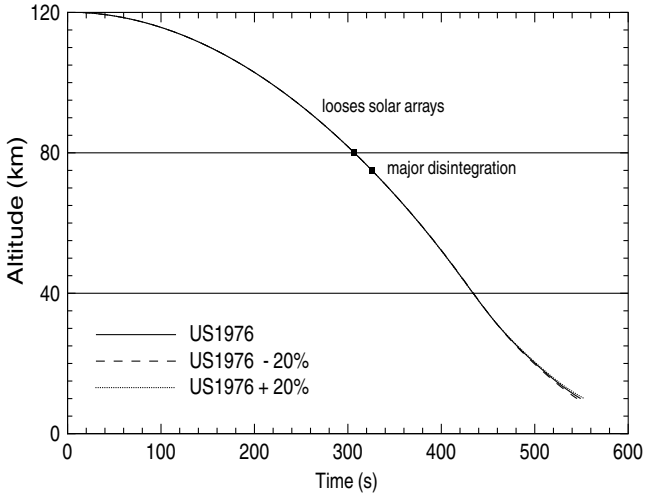

Fig. 2 Altitude evolution versus time for several atmosphere models (U.S. 1976 standard and +/− 20% of density).

displayed in Fig. 2. The altitude decreases slowly due to a very small entry path angle of −0.0085 deg.

Validity of the Approach

During the destructive reentry of the ATV, at the beginning of the destruction, the high level of heat flux might produce a fissure of the structure, most probably located at the front part of the vehicle. In this study, because the approach is axisymmetric, this perforation is modeled by an annular shaped hole. The size of the hole has been fixed arbitrarily with a difference of 20 cm between its outer an inner radii. This corresponds to a quite large area with a total surface of 1.77 m^2.

To estimate the filling time of the vehicle, the flow is modeled as in Fig. 3, where the ATV perforated structure is schematized. The supersonic flow is first decelerated to subsonic regime when crossing the shock, the two flow regimes are distinguished at the leakage. In the initial phase of the filling process a choked flow occurs, then a subsonic flow when the internal pressure is high enough. In Fig. 3 the indices 1, 2, *, and 3 refer to the variables upstream of the shock, downstream of the shock, at the fissure, and inside the vehicle, respectively. Knowing the values of the flow variables upstream of the shock, the normal shock relations [19,20] are used to provide the values of the temperature and density as well as the static and dynamic pressures downstream of the shock. The following set of equations, valid for the isentropic flow of a perfect gas, is obtained:

$$\frac{P_2}{P_1} = \frac{2\gamma}{\gamma+1}M_1^2 - \frac{\gamma-1}{\gamma+1} \tag{1}$$

$$\frac{T_2}{T_1} = \frac{\{1+[(\gamma-1)/2]M_1^2\}\{[2\gamma/(\gamma-1)]M_1^2-1\}}{[(\gamma+1)^2/2(\gamma-1)]M_1^2} \tag{2}$$

which can be rearranged as

$$\frac{T_2}{T_1} = \left(\frac{2\gamma}{\gamma+1}M_1^2 - \frac{\gamma-1}{\gamma+1}\right)\left(\frac{\gamma-1}{\gamma+1} + \frac{2}{(\gamma+1)M_1^2}\right) \tag{3}$$

Using the perfect gas law, the density ratio across the shock is

$$\frac{\rho_2}{\rho_1} = \frac{p_2/p_1}{T_2/T_1} \tag{4}$$

From Eqs. (1) and (3) the density can be expressed as a function of γ and M_1,

$$\frac{\rho_2}{\rho_1} = \frac{(\gamma+1)M_1^2}{2+(\gamma-1)M_1^2} \tag{5}$$

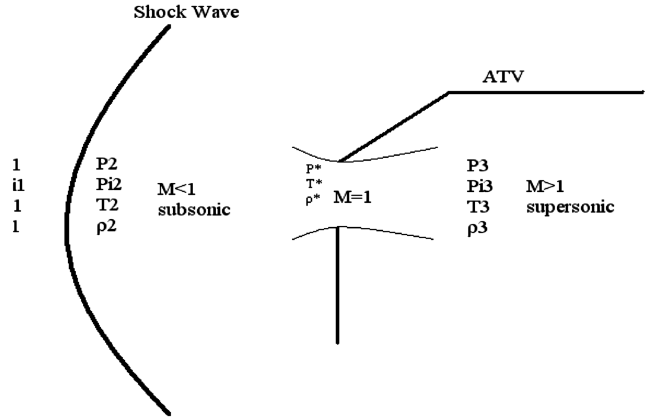

Fig. 3 Sketch of the flow through the fissure with the incoming flow, the fissured vehicle, and a virtual Laval nozzle at the fissure.

It is interesting to express the ratio between the static and dynamic pressures and temperatures across the shock. We have

$$\frac{P_{i2}}{P_2} = \left(1+\frac{\gamma-1}{2}M_2^2\right)^{\frac{\gamma}{\gamma-1}} \tag{6}$$

where the Mach number after the shock M_2 is given by

$$M_2^2 = \frac{M_1^2+[2/(\gamma-1)]}{[2\gamma/(\gamma-1)]M_1^2-1} \tag{7}$$

that can be rearranged as

$$M_2^2 = \frac{(\gamma-1)M_1^2+2}{2\gamma M_1^2-(\gamma-1)} \tag{8}$$

Finally using Eqs. (1), (6), and (8), the following expression is obtained for the ratio between the stagnation pressure downstream of the shock and the static pressure upstream of the shock as function of the upstream Mach number:

$$\frac{P_{i2}}{P_1} = \left(\frac{\gamma+1}{2}\right)M_1^2\left(\frac{[(\gamma+1)/2]M_1^2}{[2\gamma/(\gamma+1)]M_1^2-[(\gamma-1)/(\gamma+1)]}\right)^{\frac{1}{\gamma-1}} \tag{9}$$

The ratio between the dynamic and static temperatures downstream of the shock is,

$$\frac{T_{i2}}{T_2} = 1+\frac{\gamma-1}{2}\left(\frac{(\gamma-1)M_1^2+2}{2\gamma M_1^2-(\gamma-1)}\right)^2 \tag{10}$$

From Eqs. (3) and (10), the ratio between the stagnation temperature downstream of the shock and the upstream static temperature T_{i2}/T_1 is expressed as,

$$\frac{T_{i2}}{T_1} = \left(\frac{2\gamma}{\gamma+1}M_1^2 - \frac{\gamma-1}{\gamma+1}\right)\left(\frac{\gamma-1}{\gamma+1}+\frac{2}{(\gamma+1)M_1^2}\right) \times\left[1+\frac{\gamma-1}{2}\left(\frac{(\gamma-1)M_1^2+2}{2\gamma M_1^2-(\gamma-1)}\right)^2\right] \tag{11}$$

Using these equations, the values of the static and dynamic pressures and temperatures downstream of the shock have been computed and their values are reported in Table 2.

Downstream of the shock, the flow is subsonic and the pressure gradient from the shock layer toward the vehicle is large. Here the flow through the fissure is modeled as an isentropic flow in a convergent divergent nozzle. The flow is sonic at the throat located at the fissure and then becomes supersonic inside the vehicle. Therefore at the fissure, the flow variables can be expressed as a function of their stagnation values, under the hypothesis of an isentropic flow and a sonic Mach number:

Table 2 Values of the temperature and pressure upstream and downstream of the shock (indices 1 and 2, respectively) and at the fissure (*) for an altitude of 75 km. The stagnation values are denoted *i*; the upstream Mach number is 24.8

Indice	1	2	*i*2	*
Pressure, Pa	2.35	1685.84	1710.45	903
Temperature, K	208	25,072	25,176	20,979

$$\frac{P_{i2}}{P_*} = \left(1 + \frac{\gamma - 1}{2}\right)^{\frac{\gamma}{\gamma-1}} \tag{12}$$

$$\frac{T_{i2}}{T_*} = 1 + \frac{\gamma - 1}{2} \tag{13}$$

$$\frac{\rho_{i2}}{\rho_*} = \left(1 + \frac{\gamma - 1}{2}\right)^{\frac{1}{\gamma-1}} \tag{14}$$

As the fissure the mass flow rate can be expressed as

$$\dot{m}_* = A_* \rho_* c_* \tag{15}$$

where A_* is the area of the fissure. The sound speed c_* is given by

$$c_* = \sqrt{\frac{\gamma p_*}{\rho_*}} \tag{16}$$

Using Eqs. (12–14) and (16), the following expression is obtained for the mass flow rate:

$$\dot{m}_* = A_* P_{i2} \left(\frac{\gamma}{rT_{i2}}\right)^{1/2} \left(\frac{\gamma + 1}{2}\right)^{\frac{-(\gamma+1)}{2(\gamma-1)}} \tag{17}$$

where $r = R/\mathrm{M}$ with $R = 8.314\ \mathrm{J \cdot K^{-1} \cdot mol^{-1}}$ and M is the molar mass of air.

The fissure is supposed to act as the throat of a Laval nozzle. At the fissure opening the ratio between the pressure at the throat and the total pressure upstream of the throat is higher than the ratio between the total pressures downstream and upstream of the throat, we have

$$\frac{P_*}{P_{i2}} > \frac{P_{i3}}{P_{i2}} \tag{18}$$

In the first phase of the ATV filling by the external air plasma, downstream of the fissure the flow Mach number increases, becomes supersonic, and a shock wave appears. This shock wave produces a recompression associated with a deceleration of the flow. Because the gas cannot leave the vehicle, after some time the total pressure increases inside the vehicle, the Mach number decreases, and the shock wave moves toward the fissure.

As a consequence, the computation of the time necessary to fill the ATV is done in two steps. The first one corresponds to the fissure opening and lasts until the inequality of Eq. (18) is no more valid. During this phase, the mass flow rate is constant with a value of 0.77 kg/s determined using Eq. (17) and the total pressure and temperature reported in Table 2. This phase ends when Eq. (18) becomes an equality, and so when the total pressure across the fissure reaches a value of 0.53. The second phase lasts until the ratio between the total pressures outside and inside the vehicle reaches a value of 1.

The calculation of the time duration corresponding to the second phase is carried out in the following way. When the inequality of Eq. (18) is suppressed, Eq. (12) is no more valid and the Mach number is subsonic. From a Mach number of 1 to 0 with a step of 0.001, the mass flow rate is computed, then the pressure and the density. For the step j we have

$$\dot{m}_j = A_* P_{i2} \left(\frac{\gamma}{rT_{i2}}\right)^{1/2} \left(\frac{1 + \gamma + 1}{2M_j^2}\right)^{\frac{-(\gamma+1)}{2(\gamma-1)}} \tag{19}$$

$$\frac{P_{i2}}{P_j} = \left(1 + \frac{\gamma - 1}{2} M_j^2\right)^{\frac{\gamma}{\gamma-1}} \tag{20}$$

$$\frac{\rho_{i2}}{\rho_j} = \left(1 + \frac{\gamma - 1}{2} M_j^2\right)^{\frac{1}{\gamma-1}} \tag{21}$$

From the variation of the density between two consecutive steps a time dt_j is obtained,

$$\mathrm{d}\, t_j = V \frac{\rho_{j+1} - \rho_j}{\dot{m}_j} \tag{22}$$

where V is the volume of the vehicle.

The time duration of the second phase is

$$t_2 = \sum \mathrm{d}t_j \tag{23}$$

The total time to fill the ATV is obtained with a value of 0.5 s at 75 km of altitude. This corresponds for the vehicle to an altitude change of 200 m (see Fig. 2) and a change in the thermodynamic characteristics of the atmosphere lower than 5%. These very small changes in altitude and atmospheric conditions are due to the small entry path angle. Considering these results, it is possible to assimilate the reentry of the ATV to a series of static states.

Numerical Solver

The code TAU [12], developed by DLR, has been used for the numerical simulations of the ATV, with and without a perforated structure. This code solves the three-dimensional Navier–Stokes equations, written in a conservative form, with a finite volume approach. It can handle structured, unstructured, and hybrid meshes built with prisms, pyramids, tetrahedra, and hexahedra. Different numerical schemes are available for the flux discretization using upwind [advection upstream splitting method scheme (AUSM), Roe, Van Leer] or central discretization (scalar or matrix dissipation). Dissipation terms are added to damp high frequency oscillations. For the current study, the advection upstream splitting method–difference vector splitting-biased scheme (AUSM-DV) has been selected. The final scheme is accurate to the second order in space and to the first order in time. The integration in time is carried out through an explicit multistep Runge–Kutta scheme (without preconditioning). For accelerating the convergence, techniques such as local time stepping, residual smoothing, and multigrid are available. They have been used for the current computations. Transition modeling as well as different turbulence classical models and large eddy simulation are incorporated in the code. Additional numerical techniques, such as chimera and low Mach number preconditioning, are also implemented in the code. A module for grid adaptation is also available and has been used to check the grid dependence of the results. This tool is vectorized and parallelized.

This code has been extensively used and validated for the numerical simulations of hypersonic flows. Different studies have been performed for a broad range of applications including, among others, reentry flows [21], high supersonic missiles [22], and fluid-structure interaction for thermal protection systems [23].

The chemical nonequilibrium is accounted for through a 5 species (N_2, N, O_2, O, NO) and 17 equations air model [24,25]. In this model, the ionization is not taken in consideration but this phenomenon does not have a major influence for an Earth suborbital reentry. Thermodynamic and transport properties have been modeled according to the works of Eucken [26] and Wilkes [27].

Uncontrolled Propellant Ignition During Reentry

Three propellants can be present onboard the ATV during its reentry into the atmosphere: the hydrazine derivatives monomethyl hydrazine (MMH) and dimethyl hydrazine (UDMH), which are used as fuels, and nitrogen tetroxide, NTO (N_2O_4), which is an oxidizer. The remaining propellants can be either residual or unused propellants in the case of an incomplete docking to ISS. During the disintegration of the spacecraft, hypergolic fuels are released in an uncontrolled way, and then they get in contact with the hot reentry flow environment. Whether or not this actually leads to the ignition and explosive destruction of the spacecraft depends on a variety of parameters such as the following:

1) The thermodynamic state of released propellants: gaseous/liquid, temperature, pressure;

2) The flow environment: composition, temperature, pressure, velocity, and presence of hot metallic surfaces;

3) The location, mode, and rate of propellant release: valve leakage, pipe rupture, or tank bursting;

4) The ignition characteristics: autoignition temperature, minimum ignition pressure, and delay times;

5) The coupling effects: impact of blast wave or fragments on piping and tanks.

Depending on the propellant release and mixing processes, the following chemical reactions are possible:

$$\mathrm{MMH} + \mathrm{O_2} \tag{24}$$

$$\mathrm{MMH} + \mathrm{N_2O_4/NO_2} \tag{25}$$

$$\mathrm{UDMH} + \mathrm{N_2O_4/NO_2} \tag{26}$$

The purpose of this study is to assess the probability of propellant ignition and explosion associated to these gas phase reactions, taking into account the various scenarios of propellants released into the flow during reentry. This task has been carried out using the data available in the literature.

The ignition of MMH and UDMH in pure air or air contaminated with N_2O_4 and/or NO_2 at atmospheric pressures has already been studied extensively. This is due to the widespread use of these propellants and the need for definitions of safety data concerning propellant handling. As an example, Schmidt [13] mentions one incident in which a Titan II missile, operated with Aerozine 50 and NTO, exploded in its silo due to a propellant leak. Typical safety data of MMH and UDMH are summarized in Table 3. The flash point denotes the lowest temperature at which the combustible fluid can form an ignitable mixture with air. The autoignition temperature is the minimum temperature at which the mixture ignites spontaneously and produces a flame with or without the presence of an oxidizer (usually air). It depends on the composition and pressure of the combustible vapor, on the type of hot surface present, and on the amount of confinement, if the vessel is vented or not. Generally, autoignition tests are conducted at an atmospheric pressure with stoichiometric mixtures. The minimum ignition pressure and the range of flammability depend strongly on the temperature of the mixture. The quoted values are the absolute minimum ignition pressure and the maximum range of volume concentration [13]. A contamination of air with strong oxidizers, either by onboard NTO (dissociates into NO_2 in gas phase) or by dissociation of oxygen, decreases drastically the autoignition limits as shown in Fig. 4.

Table 3 Flammability data of liquid hydrazine and derivatives in pure air at atmospheric pressure [13]

	MMH	UDMH
Flash point T, K	294	258
Autoignition T, K	467	523
Minimum ignition pressure P, Pa	3.14	4
Range of flammability X, %	2.5–98	2–95

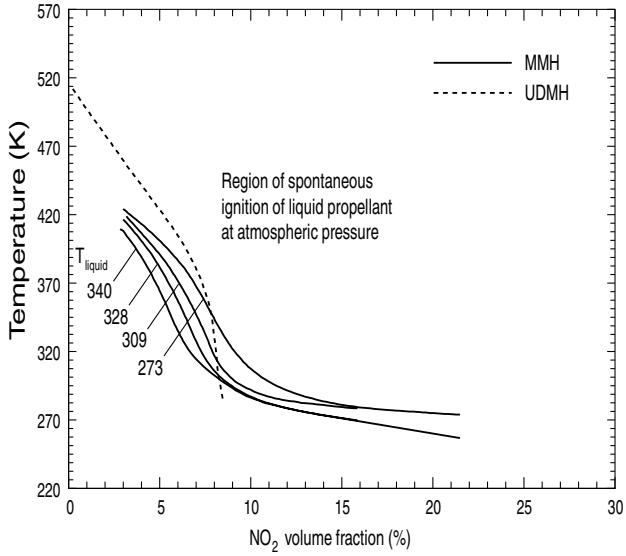

Fig. 4 Minimum autoignition temperatures of MMH and UDMH in air/NO_2 mixtures at atmospheric pressure [15].

However the flow conditions during reentry are far from the validity range of typical propellant safety data. At about 80 km of altitude, the stagnation pressure reaches a value of 1000 Pa, the stagnation temperature is above 10,000 K, and the degree of dissociation of oxygen at the stagnation point is up to 30%. Most of the literature data on propellant ignition in low pressure environments are available for the hydrazine derivatives mixed with air and nitrogen tetroxide/dioxide, respectively. A major application background is the reignition of the storable propellant propulsion system in space [9,28]. Some data are available for the reaction with molecular oxygen and little data are available on the reaction with atomic oxygen, which is considered to be highly reactive and thus will decrease the limits of ignition.

Neglecting in a first step the specific mechanisms of propellant release and mixing, a quantitative model of the autoignition limits is formulated in the section focusing on explosion analysis. The correlations derived from experimental data are then used in conjunction with trajectory and CFD data to determine the potential of onboard propellant ignition and explosion of the spacecraft.

Flow Simulations

Computational Conditions

Computations have been undertaken for the two trajectory points corresponding to the altitudes of 75 and 80 km. The flow conditions for the two points in terms of velocity, pressure, density, and temperature are reported in Table 1. No angle of attack has been accounted for; therefore axisymmetric computations have been performed. Because the ATV has a complicated shape, shown in Fig. 1, a simplified geometry, depicted in Fig. 5, has been used for the numerical simulations. In a first step, computations have been performed for the nominal ATV without structure perforation. The most probable location of the perforation has been derived from the location of the peak of heat flux on the vehicle surface. Then new computations have been performed accounting for structure perforation. For all the calculations, because the external shell of the vehicle is made with aluminum, an isothermal catalytic wall at 800 K has been applied as the boundary condition.

The meshes used for the computations have been generated using CENTAUR [29]; this software produces hybrid meshes built, for two-dimensional cases, of triangles and quadrilaterals. For both cases (intact and perforated vehicle body) an initial mesh has been

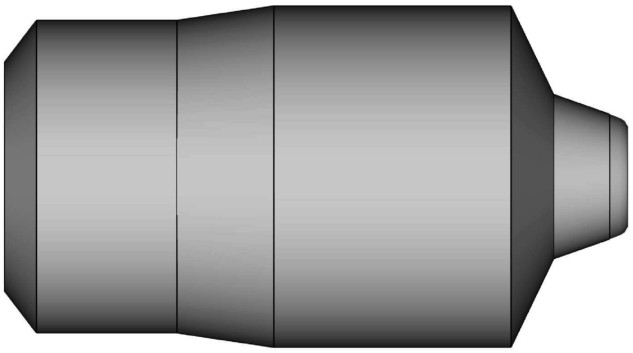

Fig. 5 Scheme of the ATV simplified geometry used for the numerical simulations.

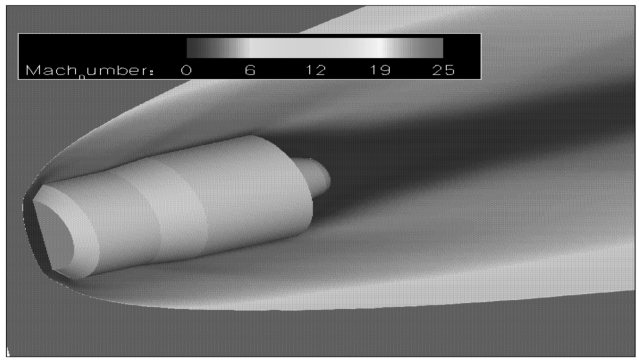

Fig. 8 Mach number distribution for an altitude of 75 km (no angle of attack).

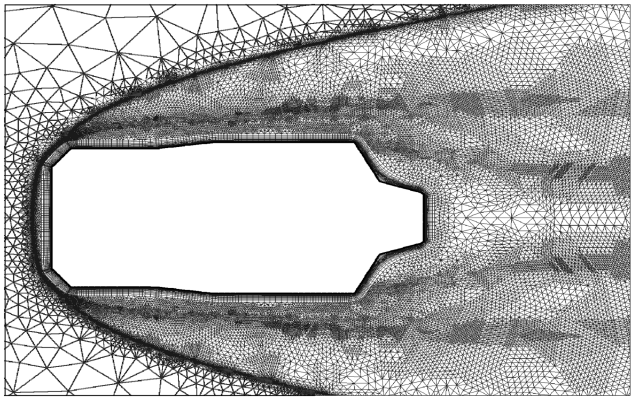

Fig. 6 Meshes used for the computations of the flowfield without and with perforation of the ATV structure at 75 km altitude.

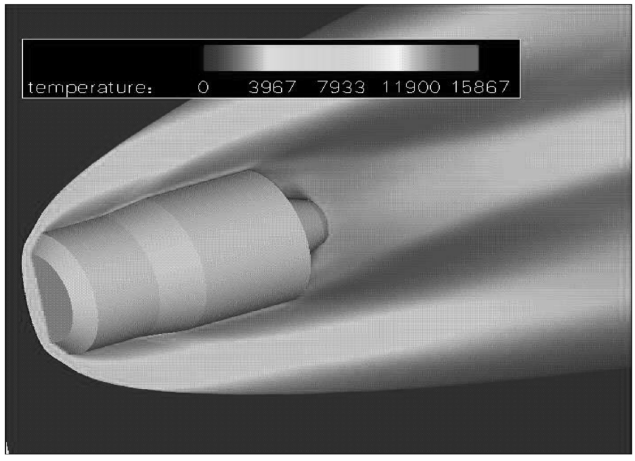

Fig. 9 Temperature distribution for an altitude of 75 km (no angle of attack).

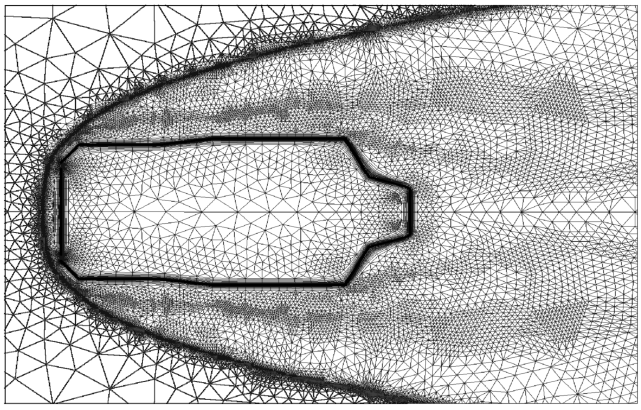

Fig. 7 Meshes used for the computations of the flowfield without and with perforation of the ATV structure at 75 km altitude.

made and then adapted with the adaptation module of TAU by adding 10% more points at each adaptation loop. With TAU, the process of adaptation is performed by adding the new mesh elements in the zones of large density gradients. The adaptation process has been stopped when the grid convergence was reached. For the cases of the intact vehicle, after seven adaptations the drag was quasi the same with a variation of about 0.05% between two consecutive loops. The mesh of the boundary layer has been adapted to have a value of y^+ lower than one. The final meshes for the geometry without and with a perforated structure, shown in Figs. 6 and 7 , are 40,000 and 42,000 elements, respectively. For the vehicle with a perforated structure, the computations showed that the maximum heat flux occurs at the first edge of the vehicle geometry. As a consequence, at this hot spot the fissure is expected. Here the size of the fissure is 20 cm and has been fixed in an arbitrary way. Because the computations are axisymmetric, the fissure has an annular shape and its surface is quite large.

The numerical simulations are initiated with an accuracy to the first order in space, then after several thousands of iterations the scheme is switched to the second order. This allows a better stability of the numerical scheme in the early ages of the calculations. The computations are initiated with a small CFL number that is then increased till a value of 1.5. The convergence is reached in approximately 50,000 iterations. For the cases with a perforated spacecraft, calculations were ended as soon as a residual flow through the gap was obtained.

External and Internal Flowfields

At first, computations were performed for the vehicle without perforation at the altitudes of 75 and 80 km. In Figs. 8 and 9, the Mach number and temperature distributions obtained for an altitude of 75 km around the undamaged ATV are plotted. The shock standoff is located at 44 cm from the stagnation point. There the Mach number decreases from a value of 24.8 (at 75 km of altitude) to a subsonic value behind the shock. The temperature reaches a maximum value close to 15,900 K in the shock layer. Downstream of this peak location, the temperature decreases progressively toward the surface. The temperature behavior essentially depends on the modeling of the chemical reactions occurring in the shock layer.

Figure 10 represents the surface pressure distribution along the ATV. The numbers between brackets in the figure correspond to the locations over the vehicle indicated by the same numbers in the ATV

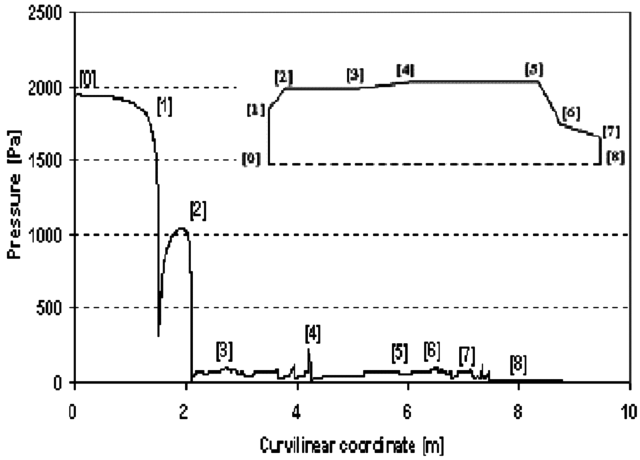

Fig. 10 Pressure distribution over the ATV for an altitude of 75 km (no angle of attack).

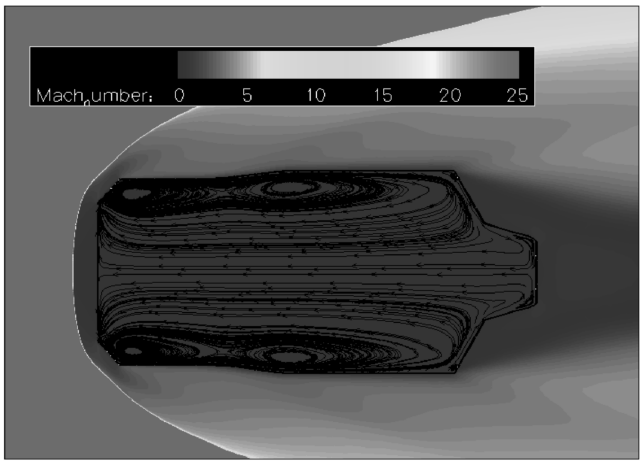

Fig. 12 Mach number distribution and streamlines inside the vehicle. Computations for an altitude of 75 km and no angle of attack.

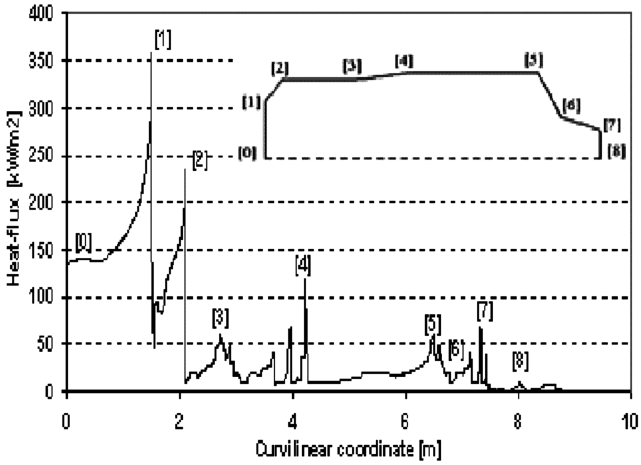

Fig. 11 Heat-flux distributions over the ATV for an altitude of 75 km (no angle of attack).

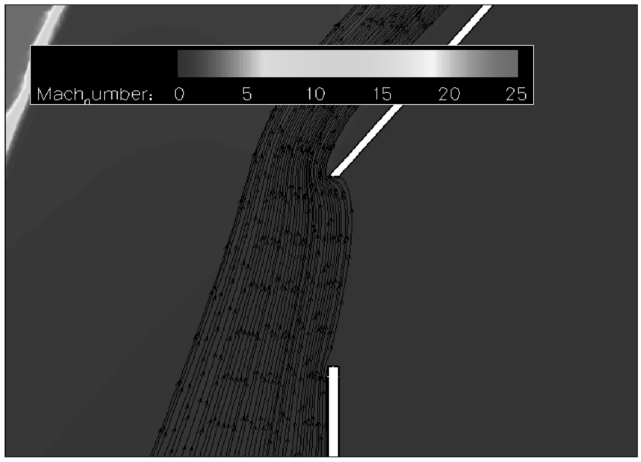

Fig. 13 Zoom of the flow at the fissure with the streamlines and the Mach number distribution.

sketch plotted in the same figure. The maximum of pressure is located at the stagnation point with a value of 1950 Pa. It decreases progressively along the surface and after the first edge the value remains still high, close to 1050 Pa. Downstream of the second edge, the pressure is very low and even negligible.

The maximum of heat flux (see Fig. 11) is of 360 kW/m^2 and is located at the first edge (location [1]) of the vehicle and not at the stagnation point. This is a consequence of the geometry of ATV with a wall perpendicular to the flow and a sharp edge. For this study, the structure of the vehicle is supposed, from a thermal aspect, to be uniform and the heat flux is assumed to be the main cause of damage. Because the maximum of heat flux is located at the first edge, in the computations accounting for a fissure, the perforation of the structure has been located there.

Then the geometry has been computed with a perforation of the structure. The internal flow is shown in Fig. 12, where the streamlines inside the vehicle and the Mach number distribution at an altitude of 75 km are plotted. The converged solution shows only a residual internal flow with a Mach number of the order of 0.01. This limit of 0.01 for the Mach number corresponds to the preconditioning available with the code. The streamline representation puts in evidence that inside the ATV a residual recirculation is present and the flow is not completely homogeneous with a weak motion. Because the computations were performed for a steady state, the pressure inside the ATV is equal to the pressure within the shock layer. As a consequence, at the convergence of the simulations there is little exchange between the two sides of the fissure. This is highlighted in Fig. 13, showing a zoom of the fissure, where no exchange is observed across the perforation. The streamlines come from the stagnation region, where the high levels of pressure are located, and pass by the fissure without penetrating inside the vehicle.

In Fig. 14, the pressure distribution around and inside the vehicle is plotted. The pressure inside the ATV is of 1790 Pa. It is nearly constant inside the vehicle and equal to the pressure of the shock layer outside the fissure. At the stagnation point, the pressure is maximum with a value of 1930 Pa. This difference of pressure makes obvious the flow direction, from the high levels of pressure to the lower ones. In Fig. 15 the heat-flux distribution along the inside structure of ATV is plotted. The maximum intensity is around 500 kW/m^2 and is located at the top part of the fissure (location [1] in Fig. 16). The maximum of surface pressure is located at the same place and reaches a value of 1950 Pa (see Fig. 16). However the surface pressure distribution is constant in all the rest of the inner structure and is equal to 1790 Pa, whereas the heat-flux distribution is changing according to the geometry.

The temperature distribution is plotted in Fig. 17. The temperature inside the ATV is quasi uniform with a value close to 1300 K. The temperature distribution has a direct effect on the partial pressures of atomic and diatomic oxygen. The dissociation of molecular oxygen starts at a temperature of 2500 K. The level of atomic oxygen represents a high interest because this element is highly reactive and its level can have an important impact on the bursting phenomenon. The partial pressure of atomic oxygen reaches a level of 630 Pa but at

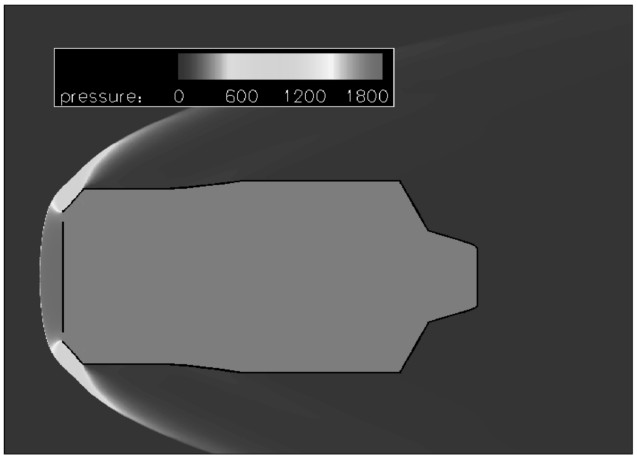

Fig. 14 Distribution of pressure around and within ATV for an altitude of 75 km and no angle of attack.

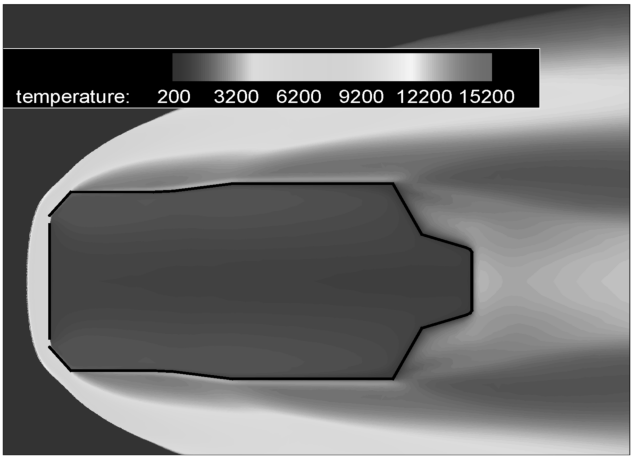

Fig. 17 Distribution of temperature around and within ATV for an altitude of 75 km and no angle of attack.

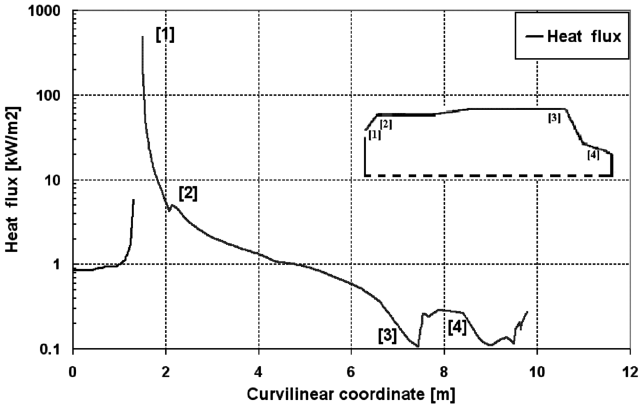

Fig. 15 Distribution of heat flux within ATV for an altitude of 75 km and no angle of attack.

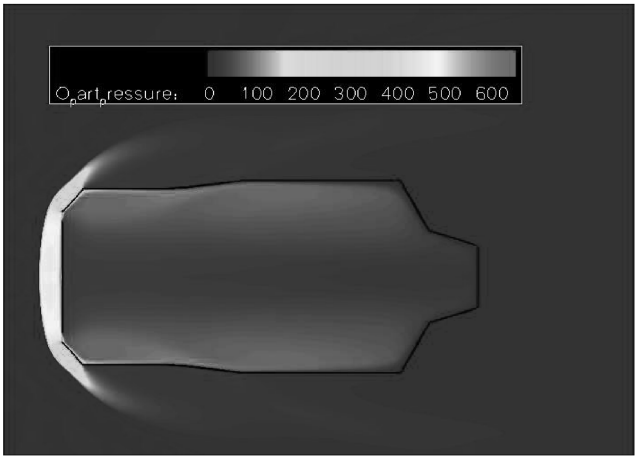

Fig. 18 Distribution of atomic oxygen for an altitude of 75 km and no angle of attack.

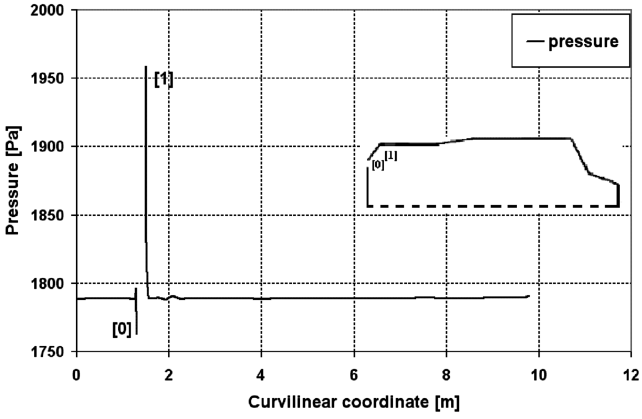

Fig. 16 Distribution of surface pressure within ATV for an altitude of 75 km and no angle of attack.

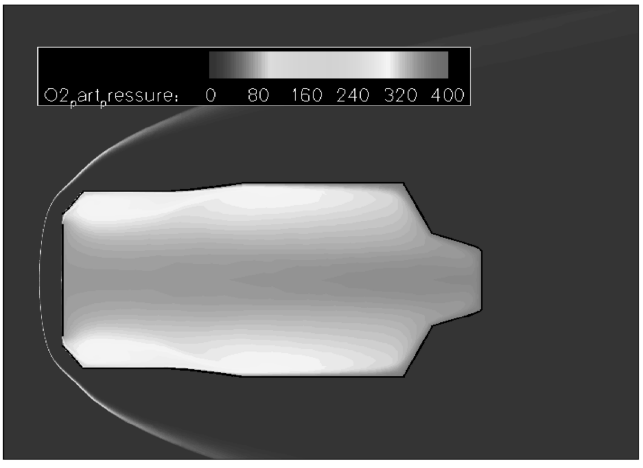

Fig. 19 Distribution of diatomic oxygen for an altitude of 75 km and no angle of attack.

the stagnation point. This is shown in Fig. 18 representing the distribution of atomic oxygen inside and outside the ATV. In fact, the atomic oxygen coming inside the ATV recombines in diatomic oxygen because the temperature is not high enough. As a consequence, the partial pressure of diatomic oxygen is much higher as shown in Fig. 19 where the partial pressure of diatomic oxygen is displayed. With the selected approach, there is little atomic oxygen inside the vehicle, and the partial pressure of atomic oxygen corresponding to these conditions is 50 Pa. The presence of this residual oxygen is due to the presence of a hot point (see Fig. 15) at the top part of the perforation where the temperature reaches locally 3000 K.

Because the partial pressure of atomic oxygen is very low inside the ATV, in the perspective of the explosion assessment the prediction of the level of diatomic oxygen is more useful. Its maximum partial pressure is 400 Pa and is located at the top of the fissure as shown in Fig. 16. Inside the vehicle, the pressure of

diatomic oxygen varies from 300 Pa in Fig. 16 to 350 Pa in the center with a maximum of 370 Pa at the wall. The presence of the maximum at the wall is due to the catalytic condition imposed there for the numerical simulations.

The same computations have been done for an altitude of 80 km. The flow pattern for the different quantities are similar to those observed at 75 km. The different results obtained in these numerical simulations have been exploited to assess the risk of explosion at these altitudes.

Explosion Analysis

Autoignition Correlations

The theoretical framework of explosion analysis is a set of correlations describing the autoignition properties of onboard propellants. To perform explosion analysis, the ignition conditions for the chemical reactions given by Eqs. (24–26) have been investigated using the data available in the literature. One mechanism leading to a potential explosion is the reaction between MMH and diatomic oxygen. The autoignition of a gaseous mixture of MMH with molecular oxygen has been investigated in detail [15]. The chemical reaction is the following:

$$C\,H_3NHNH_2 + \tfrac{5}{2}O_2 \rightarrow N_2 + CO_2 + 3H_2O \tag{27}$$

The corresponding enthalpy of combustion is

$$\Delta H = -1340 \text{ kJ/mol} \tag{28}$$

As illustrated in Figs. 20 and 21, Gray and Sherrington [15] specify the minimum autoignition pressure, $p_{i,\min}$ (in Pa), as a function of composition (volume concentration of MMH and temperature for a stoichiometric mixture). These dependencies can be described by the following correlations:

$$p_{i,\min} = 2248.1 - 11,810X_{\text{MMH}} + 35,372X_{\text{MMH}}^2 - 46,910X_{\text{MMH}}^3 + 24,967X_{\text{MMH}}^4 \tag{29}$$

$$p_{i,\min} = 1194.5 - 1.0313T + \frac{57,914}{T-600} \tag{30}$$

For this reaction, the minimum autoignition pressure is not affected by the presence of nitrogen [15].

Figure 22 summarizes experimental autoignition data and correlations for the reactions given by Eqs. (24–26) between hydrazine derivatives and molecular oxygen and NTO/NO_2 mixtures [10,15]. To provide data for a larger temperature range, the functional dependency of the minimum autoignition pressure is extrapolated. The analytical form of the correlations is as follows. Equation (30) can be refitted as

$$p_{i,\min} = T^2 e^{5115.5/T - 13.425} \tag{31}$$

The minimum ignition pressure for reaction (25) between MMH and NTO is given by

$$p_{i,\min} = 70T^2 e^{2100/T - 15.8} \tag{32}$$

For the reaction given by Eq. (26) between UDMH and NTO we have

$$p_{i,\min} = 133.3T^2 e^{1811.6/T - 16.3136} \tag{33}$$

For these three relations, the pressure is in Pa.

An important property is the ignition delay of these reactions. According to Gray and Sherrington [15], for the reaction (24) the delay is reduced when the temperature increases: from 2.6 s at 648 K to 0.6 s at 778 K. Experimental correlations on ignition delay for MMH/O_2 mixtures and higher temperatures can also be found in the literature [30,31]. For the two other reactions with NTO the ignition delay has been investigated by Seamans et al. [16] and Catoire [32,33]. The correlations proposed by Catoire [32,33] have been retained. The ignition delays, t_{ign}, are given by

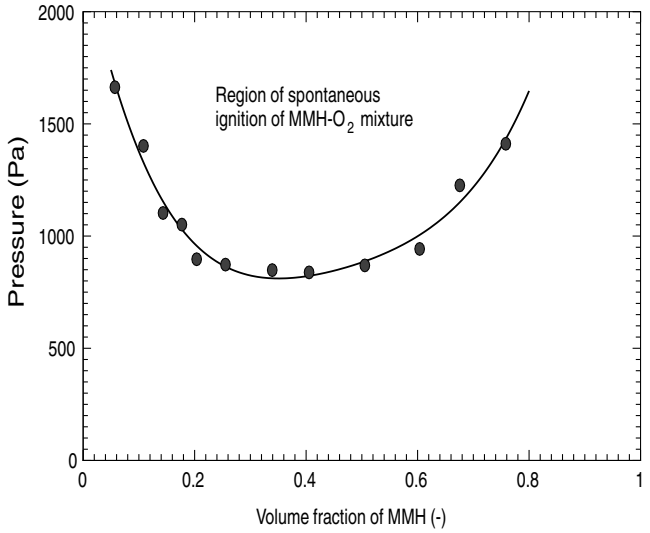

Fig. 20 Influence of mass fraction of MMH on the minimum pressure necessary to ignite reaction (24).

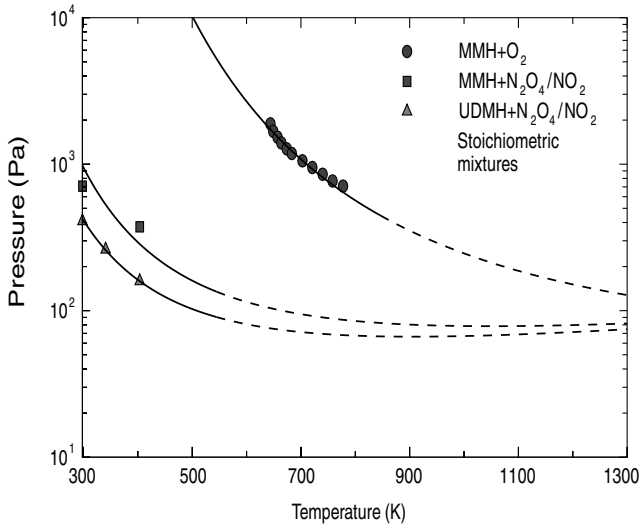

Fig. 21 Influence of temperature on the minimum pressure necessary to ignite reaction (24).

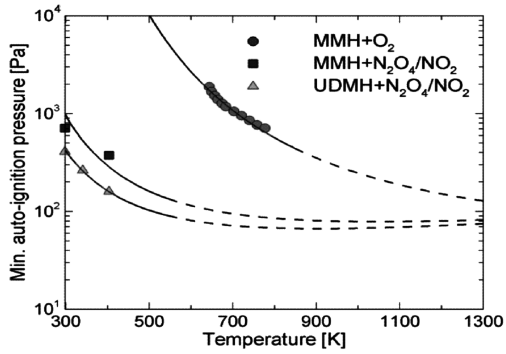

Fig. 22 Minimum autoignition pressure of different reaction sets. Experimental data from [10,15]; dashed lines extrapolated behavior.

Table 4 Summary of the main results of the numerical predictions for the two selected trajectory points (Max is the maximum value)

Altitude, km	75		80	
Flow region	External	Internal	External	Internal
Max. velocity, m/s	7200	7	7175	7
Max. temperature, K	15,720	1100	15,390	1300
Max. pressure, Pa	930	840	1930	1790
Max. O partial pressure, Pa	300	20	630	50
Max. O_2 partial pressure, Pa	188	174	390	370
Max. heat flux, kW/m^2	230	330	360	500

$$t_{\text{ign}} \frac{p^2}{T^4} = 3.0410^{-20} e^{4550/T} \tag{34}$$

$$t_{\text{ign}} \frac{p^2}{T^4} = 1.9510^{-20} e^{3260/T} \tag{35}$$

where t_{ign} is in s, p in atm, and T in K.

Coupling with CFD

Table 4 summarizes the main results obtained for the numerical simulations at 75 and 80 km of altitude. It is worth noting that there is a factor of 2 between the pressures for a difference of 5 km in altitude. This is due to the dependency of the dynamic pressure on the atmosphere evolution in terms of pressure and density. The CFD results have been exploited to assess the risk of explosion at these altitudes. Based on the computed pressure and temperature distributions in the external and internal flowfields, the correlations to determine the minimum autoignition pressures can be employed to assess whether a release of MMH or UDMH alone or with an additional release of the oxidizer, which is NTO, can lead to a local ignition of the mixture. Because the pressure and temperature distributions inside ATV are nearly homogeneous, averaged values for pressure and temperature can be used for the explosion analysis.

Figure 23 shows how the various characteristic pressure values are evolving for a decreasing altitude. As indication for the whole trajectory, the maximum of pressure computed by the trajectory analysis [11] is plotted for two different ballistic coefficients. Down to an altitude of about h = 65 km, the maximum pressure resulting from the trajectory analysis [11] is not affected by the ballistic coefficient. The pressure levels predicted by the trajectory analysis somewhat overestimate the maximum external and internal pressure resulting from the CFD simulations performed for the altitudes of 75 and 80 km. Making use of the computed maximum temperatures summarized in Table 4., the minimum autoignition pressures are evaluated and included in Fig. 23. It is obvious that $p_{\text{ign,min}}$ is roughly 1 order of magnitude below the maximum pressure level at the two altitudes. Thus a leak of MMH or UDMH inside the ATV in the presence of a perforation will ignite to the contact with molecular oxygen, which will potentially trigger an explosion of the vehicle. A simultaneous leak of NTO intensifies this effect as well as the presence of residual atomic oxygen.

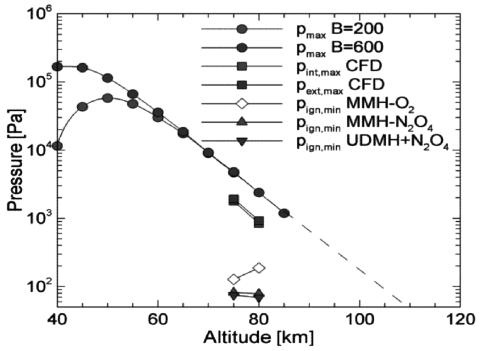

Fig. 23 Pressure data from trajectory analysis [10], CFD simulation and autoignition limits.

Conclusions

The objective of this study was the assessment of the potential of an explosive destruction of ATV during its reentry, considering a propellant leakage in the presence of a structure perforation. To achieve this, an approach has been developed in which numerical flowfield predictions have been coupled to an explosion analysis. The reliability of this approach, based on steady-state calculations where the dynamic aspect of the reentry has been assessed, has been established. A first order estimate of the time necessary to fill the vehicle has been provided by an engineering method. Comparing to the time necessary to have a drastic change of the atmosphere parameters, this filling time is found to be negligible. This conclusion is used to support the validity of the steady-state approach in which the evolution of the ATV during its entry can be represented by a succession of steady states.

From the analysis of the reentry trajectory, two points have been selected to assess the risk of destruction at a altitude higher than expected. The numerical computations of the vehicle, that account for nonequilibrium effects and catalysis, have provided the heat-flux distribution over the surface, hence the most probable location of the structure perforation during reentry. And so a 20 cm fissure, generated by the melting of the spacecraft shell, has been located at the hottest spot on ATV surface. To assess the explosion risk, numerical simulations of the flow with this fissure of the vehicle structure have been undertaken for predicting the thermodynamic conditions inside the vehicle.

The simulations have provided the internal flowfield, which is at chemical equilibrium, then with a low fraction of atomic oxygen. The temperature and oxygen partial pressure are not high in the middle of the vehicle: of the order of 1300 K and 50 Pa, respectively. Close to the walls, particularly on the top part of the fissure, the heat flux and the pressure are very high: 500 kW/m^2 and 1950 Pa. There the temperature rises up to a value of 3000 K, a level high enough to start the dissociation of diatomic oxygen. Its partial pressure reaches a level of 500 Pa at this location. Furthermore the location of the perforation is very close to the propellant tanks, which could be damaged by these local high levels of heat flux and temperature. From the explosion analysis, it is clear that such conditions are favorable to an ignition of leaking onboard propellant fuels, MMH or UDMH: the partial pressure of diatomic oxygen is more than 1 order of magnitude higher than the autoignition pressure. These results show a high risk of explosion if the propellants enter in contact with the plasma flow.

As a consequence, the potential of ATV destruction at a higher altitude than expected is not negligible. However this feasibility study is only a first step to investigate with a refined analysis the destruction of ATV during its reentry. A more accurate assessment of this risk would require a more extensive investigation. Phenomena such as thermal and mechanical fluid-structure coupling should be accounted for, allowing a more accurate prediction of the perforation of the external vehicle structure on the potential effects on the propellant tanks. The applicability of the autoignition correlations for the range of pressure and temperature characteristic of the internal flow generated by the fissure would also require further investigation.

Acknowledgments

The authors wish to thank the automated transfer vehicle development teams working at the European Space Research and Technology Center and Centre National d'Etudes Spatiales Toulouse for their support. We are grateful to E. De Pasquale from ESA who has supported this activity. We also thank Hypershall Technologie Göttingen for the cooperation during the project.

References

[1] Anon., *ESA Space Debris Mitigation Handbook*, 2nd ed., Issue 1.0, edited by H. Klinkrad, ESA, Darmstadt, Germany, 3 March 2003.

[2] Koppenwallner, G., Fritsche, B., Lips, T., and Klinkrad, H., "SCARAB —a Multidisciplinary Code for Destruction Analysis of Spacecraft

During Reentry," *Proceedings of the 5th European Symposium on Aerothermodynamics for Space Vehicles*, 2004, pp. 281–288; ESA SP 503, 2004.

[3] Lips, T., Fritsche, B., Koppenwallner, G., and Klinkrad, H., "Spacecraft Destruction During Reentry: Results and Development of the SCARAB Software System," *Advances in Space Research*, Vol. 34, No. 5, 2004, pp. 1055–1060.

[4] Marraffa, L., Mazoué, F., Foucault, R., Walpot, L., Zwaal, A., and Netterfield, M., "Experimental and Numerical Assessment of Nonequilibrium NTO Condensation During ARIANE 5 EPS Venting," ESA Report, 1996.

[5] Reynier, Ph., Wesseling, P., Marraffa, L., and Giordano, D., "Numerical Investigation on Liquid Hydrazine Behaviour During Venting into Space," *Proceedings of the European Congress on Computational Methods in Applied Sciences and Engineering: ECCOMAS 2000*, edited by E. Oñate, G. Bugeda, and B. Surez, International Center for Numerical Methods in Engineering, Barcelona, 2000.

[6] Foucaud, R., d'Herbigny, F.-X., Marraffa, L., Giordano, D., and Reynier, P., "Experimental Study of the Ariane 5 Attitude Control System (SCA) Passivation," AIAA Paper 2001-2763, 2001.

[7] Reynier, Ph., Wesseling, P., Marraffa, L., and Giordano, D., "Computation of Liquid Hydrazine Depressurization with a Mach-Uniform Staggered Grid," *Flow, Turbulence and Combustion*, Vol. 66, No. 2, 2001, pp. 113–132.

[8] Mazoué, F., Walpot, L., Netterfield, M., and Marraffa, L., "Development and Validation of Nonequilibrium Solvers," AIAA Paper 96-1893, 1996.

[9] Schmehl, R., and Steelant, J., "Influence of Injection Temperature on the Preflow Phase During Startup of an Upper-Stage Rocket Engine," AIAA Paper 2004-4011, 2004.

[10] Koppenwallner, G., Fritsche, B., Lips, T., Martin, T., Francillou, L., and De Pasquale, E., "Analysis of ATV Destructive Reentry Including Explosion Events," ESA Paper SP-587, Aug. 2005.

[11] Fritsche, B., Koppenwallner, G., and Lips, T., "Re-entry Analysis for the ATV with SCARAB," Final Report Issue 2, ESOC/ESTEC Contract No 13946/99/D/CS, HTG, Hypersonic Technology Göttingen, Katlenburg–Lindau, Germany, Aug. 2001.

[12] Gerhold, T., Friedrich, O., Evans, J., and Galle, M., "Calculation of Complex Three Dimensional Configurations Employing the DLR TAU Code," AIAA Paper 97-016735, Jan. 1997.

[13] Schmidt, E. G., *Hydrazine and Its Derivatives*, 2nd ed., Wiley-Interscience, New York, 2001.

[14] Gray, P., and Spencer, M., "Thermal Explosions in the Oxidation of Hydrazine by Nitric Oxide and Nitrous Oxide," *Journal of the Chemical Society, Faraday Transactions*, Vol. 59, 1963, pp. 879–895.

[15] Gray, P., and Sherrington, M. E., "Self-Heating and Spontaneous Ignition in the Combustion of Gaseous Methylhydrazin," *Journal of the Chemical Society, Faraday Transactions I*, Vol. 70, 1974, pp. 740–751.

[16] Seamans, T. F., Vanpee, M., and Agosta, V. D., "Development of a Fundamental Model for Hypersonic Ignition in Space Ambient Engines," *AIAA Journal*, Vol. 5, No. 9, 1967, pp. 1616–1624.

[17] Schmehl, R., Reynier, Ph., Boutamine, D. E., Steelant, J., and Marraffa, L., "Computational Analysis of ATV Reentry and Explosion Assessment," *Proceedings of the European Conference for Aerospace Sciences (EUCASS)*, European Conference for Aerospace Sciences, Moscow, 2005.

[18] Boutamine, D. E., Reynier, Ph., Schmehl, R., Steelant, J., and Marraffa, L., "Computational Analysis of ATV Reentry and Explosion Assessment," ESA Working Paper 2304, Jan. 2006.

[19] Candel, S., "Mécanique des Fluides," *Cours de* 2ème *Année*, École Centrale des Arts et Manufactures, Paris, 1983.

[20] Shapiro, A. H., *The Dynamics and Thermodynamics of Compressible Fluid Flow*, Vol. 1, Ronald, New York, 1953.

[21] Reynier, P., and Marraffa, L., "Aerothermodynamics Investigations for Earth Orbital Entry Vehicles," *Proceedings of 4th International Symposium on Atmospheric Reentry Vehicles and Systems*, Association Aeronautique et Astronautique de France, Arcachon, France, 2005.

[22] Reynier, Ph., Schülein, E., and Longo, J., "Development of a Semiempirical Actuator Disc in an Unstructured Navier–Stokes Solver for Supersonic Missiles with Grid Fins," *Journal of Spacecraft and Rockets*, Vol. 43, No. 1, 2006, pp. 84–91.

[23] Mack, A., and Schäfer, R., "Fluid Structure Interaction on a Generic Body-Flap Model in Hypersonic Flow," *Journal of Spacecraft and Rockets*, Vol. 42, No. 5, 2005, pp. 769–779.

[24] Gupta, R. N., Yos, J. M., Thompson, R. A., and Lee, K.-M., "A Review of Reaction Rates and Thermodynamic and Transport Properties for an 11-Species Air Model for Chemical and Thermal Nonequilibrium Calculations to 30,000 K," NASA Reference Publication 1232, 1990.

[25] Park, C., *Nonequilibrium Hypersonic Aerothermodynamics*, Wiley, New York, 1990.

[26] Eucken, A., "Über das Wärmeleitvermögen, die Spezifische Wärme und die Innere Reibungder Gase," *Physik. Zeitschrift*, Vol. 12, No. 24, 1911, pp. 1101–1107.

[27] Wilke, C. R., "A Viscosity Equation for Gas Mixtures," *Journal of Chemical Physics*, Vol. 18, No. 162, 1950, pp. 517–519.

[28] Lecourt, R., and d'Herbigny, F. X., "MMH/NTO Injection and Ignition in Vacuum Downstream from an AESTUS Single Injection Element," *Proceedings of the 4th International Conference on Launcher Technology and Space Launcher Liquid Propulsion: Symposium on Atmospheric Reentry Vehicles and Systems*, Centre National d'Études Spatiales, Liège, Belgium, 2002.

[29] Anon., "Online Users Manual," Centaur SoftTM, 1997–2005.

[30] Catoire, L., Bassin, X., Inginoli, W., Dupré, G., and Paillard, C., "Shock Tube Study of the Effect of Nitrogen or Hydrogen on Ignition Delays in Mixtures of Monomethylhydrazine + Oxygen + Argon," *Combustion and Flame*, Vol. 109, No. 1, 1997, pp. 37–42.

[31] Catoire, L., Ludwig, T., Bassin, X., Dupré, G., and Paillard, C., "Kinetic Modeling of the Ignition Delays in Monomethylhydrazine/Oxygen/Argon Mixtures," *Proceedings of the 27th International Symposium on Combustion*, Combustion Inst., Boulder, CO, 1998, pp. 2359–2365.

[32] Catoire, L., "Mécanismes de la Décomposition Thermique et de l'Oxidation Explosive de la Momométhylhydrazine en Phase Gazeuse," Thèse de Doctorat, Université d'Orléans, France, 1995.

[33] Catoire, L., Chaumeix, N., Pichon, S., and Paillard, C., "Visualizations of Gas-Phase NTO/MMH Reactivity at Room Temperature and NTO/MMH/He Flammability Diagrams," *Journal of Propulsion and Power*, Vol. 22, No. 1, 2006, pp. 120–126.

[34] Anon., "Automated Transfer Vehicle Factsheet," EUC-ESA-FSH-003, Rev. 1.2, European Space Agency, 2003.

I. Boyd
Associate Editor